Acta Geodyn. Geomater., Vol. 21, No. 4 (216), 287–296, 2024
DOI: 10.13168/AGG.2024.0023
journal homepage: https://www.irsm.cas.cz/acta

ORIGINAL PAPER

ANALYSIS AND FORECAST OF SEA LEVEL CHANGES ALONG CHINA SEAS AND NEIGHBORING OCEAN OVER 1993–2020

Jiahui HUANG [1], Xiaoxing HE [1]*, Shunqiang HU [2], Huajiang XIONG [3], Wentao WANG [4] and Huijuan LIU [4]

[1] *Jiangxi Province Key Laboratory of Water Ecological Conservation in Headwater Regions (2023SSY02031), Jiangxi University of Science and Technology, 1958 Ke-jia Road, Ganzhou 341000, China*
[2] *Key Laboratory of Poyang Lake Wetland and Watershed Research, Ministry of Education, Jiangxi Normal University, Nanchang 330022, China*
[3] *Jiangxi Natural Resources Surveying, Mapping and Monitoring Institute, Nanchang 330009, China*
[4] *Hebei Institute of Investigation and Design of Water Conservancy and Hydropower Co., Ltd, Shijiazhuang, 050085, China*

**Corresponding author's e-mail:* xxh@jxust.edu.cn

ARTICLE INFO

Article history:
Received 20 July 2024
Accepted 23 September 2024
Available online 8 October 2024

Keywords:
Sea level change
Satellite altimetry
Tide gauge
Deep learning

ABSTRACT

Estimates and projections of sea level change are critical for coastal areas. In this work, we utilize satellite altimetry (SA) and tide gauge (TG) technologies to estimate variations in sea level, and we also evaluate the consistency of sea level changes obtained using TG and SA from 1993 to 2020. Additionally, we use deep learning models (artificial neural network (ANN), gated recurrent unit (GRU), and long short-term memory (LSTM)) to forecast sea level changes with SA time series. Our results reveal that the average absolute sea level (ASL) rate in the China Seas and the neighboring ocean based on SA is 3.55 mm/yr, which is higher than the global rate of 3.30 mm/yr. Specifically, the ASL rates of East China Sea and South China Sea are 3.21 mm/yr and 4.24 mm/yr, respectively. The sea level change in the South China Sea is significantly greater than that in the East China Sea. Secondly, the relative sea level (RSL) rate based on TGs is 3.88 mm/yr. We perform VLM correction on TGs with co-located GNSS following the method of Zhou et al. (2022) and obtain a TG-based ASL result of 3.77 mm/yr. Our results show that there is good consistency between coastal sea level changes estimated using tide gauges and satellite radar altimetry. Finally, we use the ANN, GRU, and LSTM models to predict sea level change with SA. The results show that LSTM's prediction accuracy is better than that of the other models, with average RMSE, MAE, and R^2 values of 48.92 mm, 35.99 mm, and 0.85, respectively.

1. INTRODUCTION

The Sixth Assessment Report (AR6) released by the Intergovernmental Panel on Climate Change (IPCC) states that the rate of sea level rise is accelerating (3.7 mm/yr, Tong et al., 2022), which is likely to result in irreversible phenomena (e.g., coastal inundation (Marfai and King, 2008), saltwater intrusion (Cantelon et al., 2022), or loss of coastal ecosystems (Cazenave and Cozannet, 2014)). The China Sea Level Bulletin (2020) revealed that the rise in sea levels along the coast of China accelerated in the period from 1980 to 2020, with an average rise rate of 3.4 mm/yr and an increase of 0.07 mm/yr^2. From 1993 to 2020, the sea level rise rate in China was 3.9 mm/yr (Wang et al., 2022a). This was higher than the global average of 3.3 mm/yr for the same period (Cazenave and Moreira, 2022). Rising sea levels directly threaten the economic and social development of coastal areas (Cui et al., 2018). China's coastal areas, located in the Northwest Pacific, characterized by relatively high sea level rise rates, face greater risks due to the impact of rising sea levels.

The main technologies used to monitor the sea level are TG and SA, as well as ocean profiling systems (Marcos et al., 2019; Cazenave and Remy, 2011). Numerous studies on sea level change have been conducted based on these observations. Prior to the 1990s, the monitoring of sea level change primarily relied on TG observation data distributed along the coast, which were influenced by local vertical land motion (Wöppelmann and Marcos, 2016). Qu et al. (2019) used 25 TG records to analyze sea level rise in the China Seas and estimated the local vertical land motion. The results indicated a sea level rise rate of 3.2 ± 1.1 mm/yr from 1993 to 2016. Wang et al. (2022a) analyzed the temporal and spatial characteristics of sea level change along the coast of China using TG observations over the last 60 years. An accelerated sea level rise rate was discovered, with an estimated increase of 0.07 mm/yr^2. Mu et al. (2024) used a data assimilation method that combined global TG data, climate models, and sea level fingerprints to evidence that the sea level rise rate in China from 1950 to 2020 (1.95 ± 0.33 mm/yr) was higher than the global average (1.71 ± 0.17 mm/yr) and had exhibited a significant accelerating trend since 1980. SA technology, which emerged in the late 1970s, provides a highly effective method to study global/regional sea level change. Feng et al. (2012) used SA data from 1993 to 2009 to calculate an average sea level change

Cite this article as: Huang J, He X, Hu S, Xiong H, Wang W, Liu H: Analysis and forecast of sea-level change in the China Seas and neighboring oceans from 1993 to 2020. Acta Geodyn. Geomater., 21, No. 4 (216), 287–296, 2024. DOI: 10.13168/AGG.2024.0023

Table 1 Description and locations of TG networks along the coast of the China Seas (https://psmsl.org/data/obtaining/).

Virtual Coastal Station	ID	Lon.	Lat.	Period
ZHAPO	0933	111.817	21.583	1993.0–2020.9
KANMEN	0934	121.283	28.083	1993.0–2020.9
LUSI	0979	121.617	32.133	1993.0–2020.6
NAHA	1151	127.665	26.213	1993.0–2020.9
AKUNE	1265	130.191	32.018	1993.0–2020.9
KARIYA	1318	129.849	33.473	1993.0–2020.9
OKINAWA	1388	127.824	26.179	1993.0–2020.9
QUARRY BAY	1674	114.213	22.291	1993.0–2020.9
TANJONG PAGAR	1746	103.850	1.267	1993.0–2020.9

rate of 5.5 ± 0.7 mm/yr for the South China Sea. This was significantly higher than the global sea level rise rate of 3.3 ± 0.4 mm/yr for the same period. Gou et al. (2015) used SA data from TOPEX/Poseidon, Jason-1, and Jason-2 to study the spatiotemporal changes in sea levels in the China Seas and the Western Pacific. An average sea level rise rate of 4.64 mm/yr was observed in their study area. Yuan et al. (2021) used average sea surface height data from multiple satellites over different periods to construct a high-resolution sea level trend (SLT) model. A sea level rise rate of 3.42 mm/year, higher than the global average rate of approximately 3 mm/yr, was observed in the China Seas and adjacent areas. These results all demonstrate that Chinese sea levels are rising at rates that are higher than the global average.

The AR6 also states that the global average sea level will rise by 0.44–0.76 m and 0.63–1.01 m under medium- and high-emission scenarios, respectively, by 2100, and that future global sea level rise will be irreversible on a centennial-to-millennial scale (Tong et al., 2022). Recently, many scholars have used deep learning models and regional ocean models to predict global or regional sea level change. Church and White (2011) used a time series analysis and linear regression methods to reconstruct the long-term trend of the global mean sea level (GMSL) from the late 19th to the early 21st century. To support future sea level rise predictions, they produced an accurate historical record of sea level change by separating the contributions of drivers such as thermal expansion and glacier melting. Jin et al. (2021) effectively forecasted future sea level change in the marginal seas adjacent to China using a high-resolution regional ocean model and dynamical downscaling. Balogun and Adebisi (2021) explored the use of an autoregressive integral moving average (ARIMA) model, as well as support vector regression (SVR) and long short-term memory (LSTM) neural networks, to predict sea levels. An evaluation of the performance of classical time series, machine learning, and deep learning models revealed that different prediction models were suitable for different regions. Estimating sea level rise and accurately predicting future sea level change are crucial for the sustainable development of coastal communities.

In this study, we conducted an in-depth analysis of the rise in sea levels in the China Seas and the neighboring ocean by analyzing long-term observation data from nine TG stations in combination with SA data. Different deep learning models were used to predict and compare the SA time series. Section 2 of this study introduces the data and methods. Section 3 examines the rates of sea level change using TG and SA to explore the consistency of the ASL rate obtained from two observations; it also discusses the prediction performance of different deep learning models for various SA time series. Section 4 presents the conclusions.

2. DATA AND METHODS

2.1. TIDE GAUGE DATA

The TG data used in this study were obtained from the Permanent Service for Mean Sea Level (PSMSL, https://psmsl.org/), which collects monthly observation data from nine TG stations located in the China Seas and the neighboring ocean. Additional information regarding the geographical distribution of the TG network is provided in Table 1. Figure 1 presents the spatial distribution of TG stations (red points). We obtained the Revised Local Reference (RLR) data for the period from January 1993 to December 2020 from the PSMSL website (Holgate et al., 2013; PSMSL, 2023). The average missing data rate was 3.39%. In response to this, we used the regularized expectation maximization algorithm (RegEM) to interpolate the missing data (Schneider, 2001). The nine TGs used in this study were chosen because the distance between them and the co-located GNSS stations was within approximately 20 km (the maximum distance was 20.84 km), so any relative vertical motion was minimized (the relative movements between the GNSS antennae and the TGs were assumed to be negligible) (Collilieux and Wöppelmann, 2011; Santamaría-Gómez et al., 2014; Bitharis et al., 2017). Thus, the TG and corresponding co-located GNSS data were considered to represent the same points. We also measured the spatial–temporal alignment between the TG data and the SA re-analysis data to ensure consistency in the subsequent analysis of the ASL rate. The co-located GNSS data used in this study were sourced from Zhou et al. (2022).

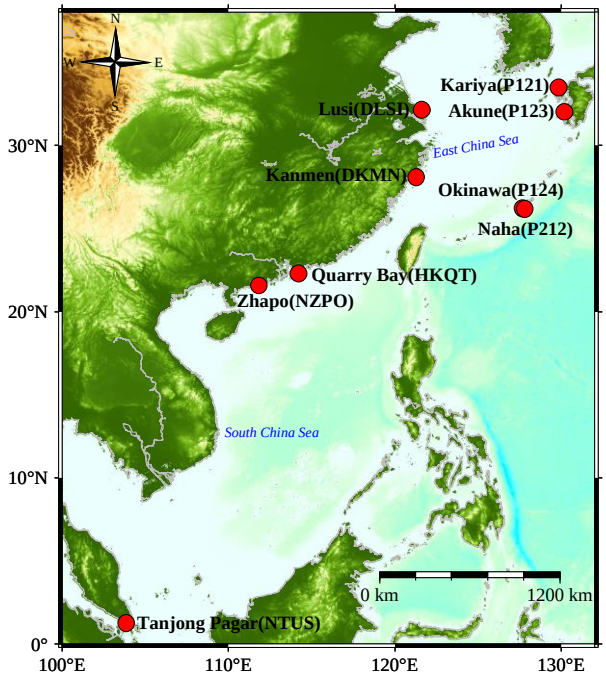

Fig. 1 Spatial distribution of tide-gauge networks (red points) and the co-located GNSS stations (in brackets).

2.2. SATELLITE ALTIMETRY RE-ANALYSIS PRODUCT

We selected the "GLOBAL_MULTIYEAR_PHY_001_030" ocean re-analysis product provided by the Copernicus Marine Environment Monitoring Service (CMEMS,https://data.marine.copernicus.eu/product/GLOBAL_MULTIYEAR_PHY_001_030/description, accessed on 04 Jul 2023). This product was defined on a regular grid with a resolution of 1/12° (approximately 8 km) and spanned 50 standard vertical levels (Aulicino et al., 2018; He et al., 2022; Huang et al., 2024). We determined the longitudes and latitudes of the SA virtual stations at the locations of the TGs, allowing us to extract the SA time series. The span of the SA time series is consistent with that of the TGs (1993–2020), with a daily resolution.

Previous research has demonstrated that the glacial isostatic adjustment (GIA) model prediction for the global average between 66°N and 66°S is -0.30 mm/yr (Peltier et al., 2015). This constant must be applied when correcting globally averaged sea level rise measured using SA to account for the impact of the GIA on absolute sea levels (Peltier, 2001; Chen et al., 2018; Wang et al., 2022b). The impact of the GIA was included in the vertical land motion (VLM) obtained from the GNSS stations (Santamaría-Gómez et al., 2014; Houston et al., 2012; Wang et al., 2021). It is important to note that GIA adjustments to SA data are necessary to ensure consistency (Zhou et al., 2022). The GIA data used for this correction were obtained from the results of the global glacial isostatic adjustment process refinement model (ICE-6G_C), developed by Professor Peltier's team at the University of Toronto (Argus et al., 2014; Peltier et al., 2015) and available at (https://www.atmosp.physics.utoronto.ca/~peltier/data.php) .

2.3. DEEP LEARNING ALGORITHMS IN FORECASTING SA TIME SERIES

In this section, we briefly introduce the three deep learning algorithms—ANN, GRU, and LSTM—used to forecast SA time series in this study.

2.3.1. ARTIFICIAL NEURAL NETWORK ALGORITHM

Artificial neural networks (ANNs) are learning models that are constructed by simulating the information-processing mechanisms of human neurons. These models provide adaptability, self-learning, and a high fault tolerance. However, the problem of vanishing gradients becomes significant as the number of hidden layers in the ANN increases (LeCun et al., 2015; Hua et al., 2019). The structure of an ANN mainly consists of several neurons connected by links. The output value of the entire network is primarily determined by the network's structure, the way the network is connected, the weight values, and the activation functions. An artificial neuron model comprises a set of weights, a threshold, and a transfer function (f). An artificial neuron model is illustrated in Figure 2.

The input vector of neuron j is $X_j = (x_1, x_2, \ldots, x_n)^T$; the input weight is $W_j = \left(w_{1j}, w_{2j}, \ldots, x_{nj}\right)^T$, and the threshold is θ_j. The input to neuron j is $S_j = \sum_{i=1}^{n} x_i w_{ij} - \theta_j$ and the output is $y_i = f\left(s_j\right)$, where f is the transfer function presented in Figure 2.

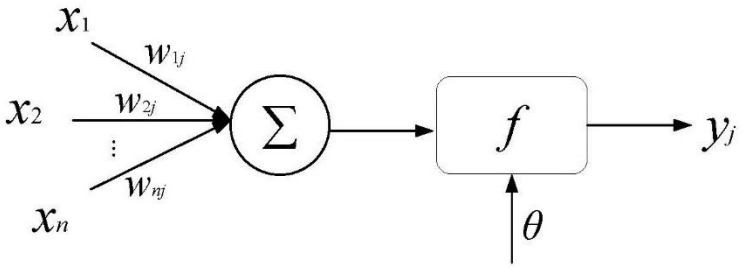

Fig. 2 The structure of an ANN model.

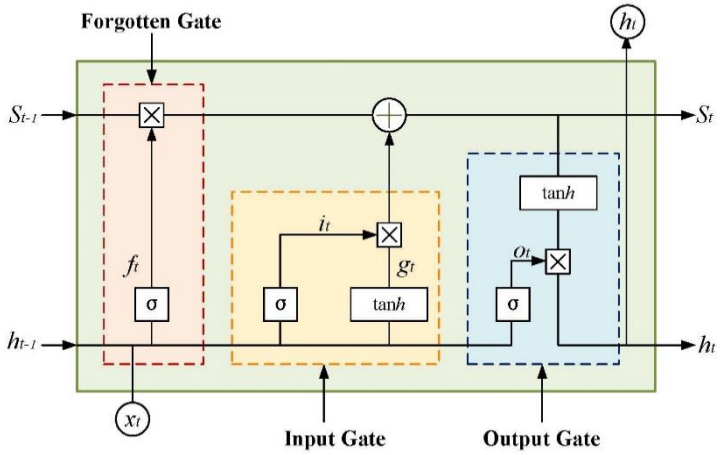

Fig. 3 Basic structure of an LSTM.

2.3.2. LONG SHORT-TERM MEMORY NEURAL NETWORK

A long short-term memory (LSTM) network is an improved type of recurrent neural network (RNN) with strong discriminative and learning capabilities. It can learn the nonlinear relationships contained in time series and, through its memory modules, it is able to address issues that occur in RNNs, such as vanishing gradients, exploding gradients, and an insufficient long-term memory capacity (Hochreiter and Schmidhuber, 1997; Song et al., 2020; Hua et al., 2019). LSTMs are widely used in the prediction of highly nonstationary time series such as sea level time series (Sun et al., 2020; Balogun and Adebisi, 2021).

The basic unit of an LSTM consists of a forget gate, an input gate, and an output gate (Yu et al., 2019; Hua et al., 2019). A detailed structure is presented in Figure 3. In the forget gate, inputx_t, state memory cell S_{t-1}, and intermediate output h_{t-1} jointly determine the portion of the state memory cell to forget. In the input gate, vectors x_t and h_{t-1} are transformed by sigmoid and tanh functions, respectively, to determine the retained vectors in the state memory cell. Intermediate output h_t is determined by updated state memory cell S_t and output O_t.

2.3.3. GATED RECURRENT UNIT

A gated recurrent unit (GRU) is a simplified LSTM model that can process sequential data such as text, speech, and time series (Cho et al., 2014). A GRU has a simpler structure and faster training speed than an LSTM and is simplified by introducing an update gate and reset gate. It may not be as flexible and effective as an LSTM when dealing with complex time series (Dey and Salem, 2017; Cahuantzi et al., 2023). Its computational expressions are presented in Equation (1).

$$\begin{cases} z_t = \sigma\left(W_z x_t + U_z h_{t-1} + b_z\right) \\ r_t = \sigma\left(W_r x_t + U_r h_{t-1} + b_r\right) \\ h_t = \tanh\left(W_h x_t + U_h\left(r_t \otimes h_{t-1}\right) + b_h\right) \\ h_t = \left(1 - z_t\right) \otimes h_{t-1} + z_t \otimes h_t \end{cases} \quad (1)$$

where $\otimes$ represents element-wise multiplication in the matrix; W_z, W_r, W_h, U_z, U_r, and U_h are the weight coefficients; b_z, b_r, and b_h are the bias terms for the input parameters; z_t and r_t are the outputs of the update gate and reset gate at time t; x_t is the input at time t; h_t is the output at time t; $\widetilde{h_t}$ is the candidate activation; and σ is the sigmoid function.

2.3.4. EVALUATION INDEX

In this study, we selected the root mean square error (RMSE), mean absolute error (MAE), and coefficient of determination (R^2) as the accuracy evaluation metrics to quantitatively assess the performance of the prediction models. Lower RMSE and MAE values correspond to a higher prediction accuracy of the model. The R^2 value ranges from 0 to 1; the closer it is to 1, the more accurate the model's predictive capability. The expressions for these metrics are as follows:

$$\begin{cases} RMSE = \sqrt{\frac{1}{n}\sum_{i=1}^{n}(y_i - \hat{y}_i)^2} \\ MAE = \frac{1}{n}\sum_{i=1}^{n}|\hat{y}_i - y_i| \\ R^2 = 1 - \frac{\sum_{i=1}^{n}(y_i - \hat{y}_i)^2}{\sum_{i=1}^{n}(y_i - \overline{y})^2} \end{cases} \quad (2)$$

where y_i represents the observed values, $\hat{y}_i$ represents the predicted values, $\overline{y}$ is the mean of the actual values of the SA time series, and n is the number of observations.

3. RESULTS AND DISCUSSION

3.1. ABSOLUTE SEA LEVEL CHANGE ALONG THE COAST OF THE CHINA SEAS BASED ON SA

Colored noise affects sea level time series, and neglecting it may introduce biases when estimating sea level rise rates (Church and White, 2011; Bos et al., 2014; Royston et al., 2018; He et al., 2022; Huang et al., 2024). We estimated the rates of nine SA time series using both white noise (WN) and autoregressive moving average (ARMA (1,1)) models. Figure 4 presents the results of the ASL rates from 1993.0 to 2020.9 obtained using the WN and ARMA (1,1) models. We obtained similar values of 3.26 and

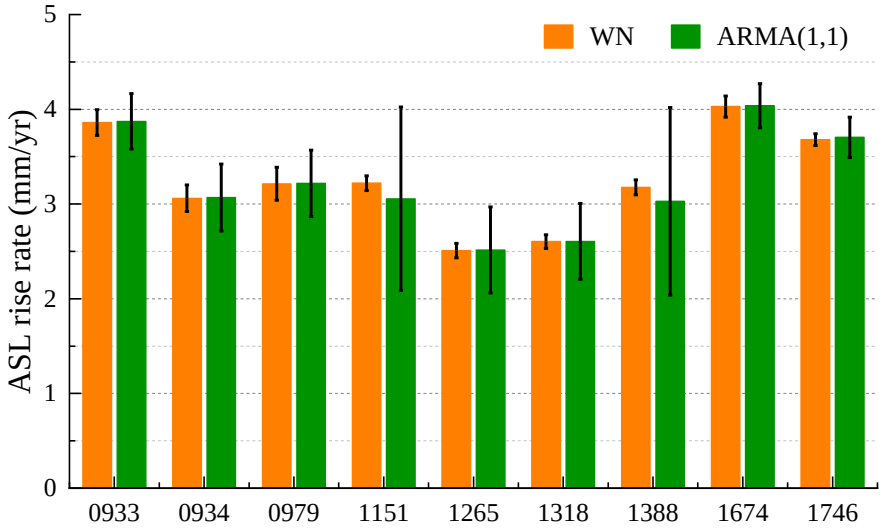

Fig. 4 ASL rates from satellite altimetry virtual stations using WN and ARMA (1,1) models (error bars represent uncertainty).

3.23 mm/yr, respectively, from both models. However, the estimates for rate uncertainties obtained by the ARMA (1,1) model were approximately 2 to 12 times higher than those from the WN model. This indicated that pure WN underestimated the uncertainty in estimating sea level rise rates, which affected the accuracy of sea level change calculations.

The ASL rates ranged from 2.81 ± 0.45 mm/yr to 4.37 ± 0.23 mm/yr across the nine SA virtual stations when using the ARMA (1,1) model (Table 2). The average ASL rate estimated in this study was 3.55 ± 0.54 mm/yr, which was higher than the global rise rate of 3.3 mm/yr for the same period (Zhou et al., 2022; Qu et al., 2019; Mu et al., 2020). Comparing our results with those of Zhou et al. (2022), the difference in the ASL rates estimated using SA from the same stations ranged from 0.30 mm/yr to 0.96 mm/yr (Figure 5). It should be noted that the distinctions in data sources, rate estimation methods, and time scales of ASL estimation between our study and that of Zhou et al. (2022) led to some inconsistencies in the results, even though they remain relatively similar. There were significant differences in the rate values between stations in different sea areas, with higher rates in the south and lower rates in the north. The mean ASL rate for the SA virtual stations near the East China Sea (KANMEN, LUSI, NAHA, AKUNE, KARIYA, and OKINAWA) was 3.21 ± 0.27 mm/yr, whereas the average for the stations near the South China Sea (ZHAPO, TANJONG PAGAR, and QUARRY BAY) was 4.24 ± 0.11 mm/yr. This indicates that the sea level rise rate in the East China Sea was lower than that in the South China Sea. The average rate in the South China Sea was higher than the sea-level rise rate for the China Seas from 1980 to 2021 (3.40 mm/yr; China Sea Level Bulletin, 2021).

3.2. RELATIVE SEA LEVEL CHANGE ALONG THE COAST OF THE CHINA SEAS BASED ON TGS

Similarly, to SA estimation we computed the RSL rate estimates using the ARMA (1,1) noise model. Table 3 presents the RSL rates from the nine TG stations for the period 1993.0–2020.9, which range from 2.46 to 7.19 mm/yr, with an average of 3.88 mm/yr. The differences in RSL range from 0.08 to 1.66 mm/yr (with an average difference of 0.43 mm/yr). This is comparatively consistent with the results of Zhou et al. (2022), who used the same TG stations. For accurate ASL change estimation, RSL must be corrected for the effect of VLM. This is addressed in the next section.

Table 2 Comparison between ASL rates (mm/yr) along the coast of the China Seas obtained from CMEMS satellite altimetry re-analysis data and the results from Zhou et al. (2022).

Station	ASL Rate [a]	ASL Rate (Zhou et al., 2022)
ZHAPO	4.24 ± 0.29	3.37 ± 0.29
KANMEN	3.44 ± 0.35	3.95 ± 0.27
LUSI	3.63 ± 0.35	3.16 ± 0.28
NAHA	3.21 ± 0.97	3.59 ± 0.32
AKUNE	2.81 ± 0.45	3.10 ± 0.22
KARIYA	3.01 ± 0.40	3.81 ± 0.22
OKINAWA	3.18 ± 0.99	3.54 ± 0.33
QUARRY BAY	4.37 ± 0.23	3.43 ± 0.29
TANJONG PAGAR	4.10 ± 0.21	3.14 ± 0.23

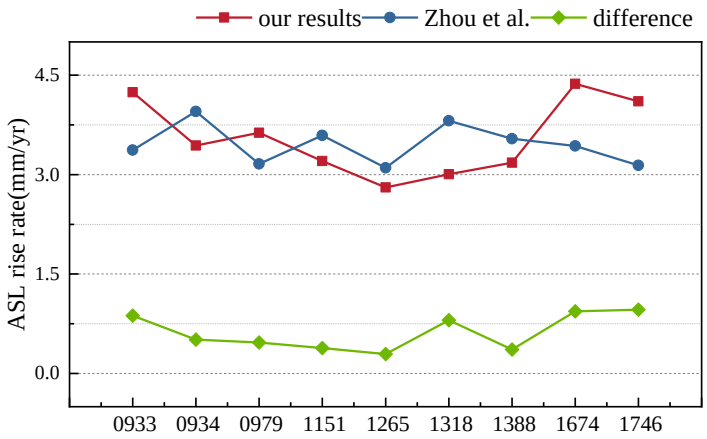

Fig. 5 Estimated rise rate at nine SA virtual stations along the coast of the China Seas: comparison between our analysis results using the ARMA (1,1) model (red) and the results from Zhou et al., 2022 (blue). The green line represents the ASL difference between the two results.

Table 3 RSL rates estimated using nine TGs (mm/yr) compared with the results from Zhou et al. (2022).

Station	RSL Rate	RSL Rate (Zhou et al., 2022)
ZHAPO	3.46 ± 1.04	3.38 ± 0.31
KANMEN	5.72 ± 1.23	5.24 ± 0.28
LUSI	7.19 ± 2.13	5.53 ± 0.31
NAHA	3.08 ± 0.68	3.30 ± 0.35
AKUNE	3.14 ± 0.45	3.08 ± 0.29
KARIYA	3.22 ± 0.90	3.51 ± 0.29
OKINAWA	3.06 ± 0.69	3.18 ± 0.33
QUARRY BAY	2.46 ± 1.00	2.73 ± 0.35
TANJONG PAGAR	3.56 ± 1.03	4.24 ± 0.28

3.3. CONSISTENCY OF THE ABSOLUTE SEA LEVEL RISE RATE USING TG AND SA DATA

An ASL change can be obtained not only from SA data but also from long-term TG records. An ASL change obtained from TG data is influenced by two factors: the VLM in the TG area obtained from co-located GNSS stations and the RSL change measured by the TGs (Montillet et al., 2018; Santamaría-Gómez et al., 2014; Zhou et al., 2022). The following formula, provided by Wöppelmann and Marcos (2016), was used to obtain the ASL from the TGs and co-located GNSS stations:

$$V_{ASL} = V_{RSL} + U \tag{3}$$

where V_{RSL} is the RSL rate obtained from the TG, U is the VLM rate obtained from the co-located GNSS stations, and V_{ASL} is the ASL rate. The uncertainty was the square root of the quadratic sum of the uncertainties of the VLM and RSL rates.

The ASL rates calculated using TG+GNSS and SA data from the nine stations over the period 1993.0–2020.9 are presented in Table 4, along with the consistency calculations. The ASL rates obtained from the TGs after VLM correction ranged from 2.31 to 5.35 mm/yr, with an average value of 3.77 ± 1.05 mm/yr. The coastal regional ASL rates estimated using GNSS+TG data were consistent with the results from the SA observation, supporting the conclusions of previous studies, such as those conducted by He et al. (2022) and Bruni et al. (2022). Table 4 depicts the differences in the ASL rates obtained from the two observations; the difference was less than 2.00 mm/yr for eight of the stations included in this study (maximum value of 2.55 mm/yr; AKUNE), and the minimum value was 0.02 mm/yr. The variation in the differences found by Zhou et al. (2022) was in the range of 0.20~2.19 mm/yr, with a mean value of 0.64 mm/yr. The mean value of the difference in our results was 0.99 mm/yr, which is in good agreement with their study.

3.4. SA TIME SERIES FORECAST ALONG THE COAST OF THE CHINA SEAS USING DEEP LEARNING ALGORITHMS

Based on the previous experimental analysis, we conclude that TG and SA are highly consistent in terms of estimating ASL rates. Both the TG and SA techniques are primary sources for monitoring global and regional sea level change, providing long-term observation records for research on historical sea level change (Cipollini et al., 2017). TG monitoring has limitations, such as limited spatial coverage, local effects (e.g., geological structures, coastal erosion), and interference from VLM (Wöppelmann and Marcos, 2016; Pugh, 2014; Douglas, 2001; Woodworth and Player, 2003). With the rapid development of SA technology, it has emerged as a key tool for future sea level monitoring, offering

Table 4 ASL rates estimated using TG+GNSS and SA data from the nine coastal stations analyzed in this study (mm/yr) compared with the results from Zhou et al. (2022).

Station	ASL Rate		Difference (Our Results)	Difference (Zhou et al., 2022)
	TG+GNSS*	SA		
ZHAPO	4.37 ± 1.27	4.24 ± 0.29	0.13 ± 1.31	0.92 ± 0.84
KANMEN	4.23 ± 1.26	3.44 ± 0.35	0.79 ± 1.31	−0.20 ± 0.48
LUSI	5.35 ± 2.15	3.63 ± 0.35	1.72 ± 2.18	0.53 ± 0.52
NAHA	3.45 ± 1.10	3.21 ± 0.97	0.25 ± 1.46	0.08 ± 0.98
AKUNE	5.35 ± 2.33	2.81 ± 0.45	2.55 ± 2.38	2.19 ± 2.32
KARIYA	3.02 ± 1.30	3.01 ± 0.40	0.02 ± 1.36	−0.50 ± 1.00
OKINAWA	3.16 ± 0.97	3.18 ± 0.99	-0.02 ± 1.39	−0.26 ± 0.83
QUARRY BAY	2.31 ± 1.43	4.37 ± 0.23	-2.06 ± 1.45	−0.85 ± 1.12
TANJONG PAGAR	2.71 ± 1.28	4.10 ± 0.21	-1.39 ± 1.30	0.25 ± 0.85
Average	3.77 ± 1.05	3.55 ± 0.53	0.22 ± 1.33	0.79 ± 0.75

VLM rate from Zhou et al. (2022)*

global coverage and higher spatial resolution (Ablain et al., 2017; Cazenave and Nerem, 2004). At the same time, forecasting future sea level trends has garnered significant attention from scholars. With advancements in artificial intelligence (AI) technology, more accurate predictive models and algorithms now provide new possibilities for precise time series forecasting. Among various AI techniques, deep learning models such as ANN, LSTM, and GRU have shown great potential for time series forecasting, including sea level prediction (Hochreiter and Schmidhuber, 1997; Rumelhart et al., 1986; Cho et al., 2014). Sea level change is influenced by complex factors and exhibits significant nonlinear characteristics, and deep learning models excel at capturing these nonlinear patterns, enabling more accurate simulations and predictions of sea level change (Balogun and Adebisi, 2021).

In this study, we forecasted SA time series with daily resolution. We adopted a common 8:1:1 split for the training, validation, and test sets, respectively, due to the large size of the dataset (Li et al., 2020; Chen et al., 2023). Specifically, the dataset was divided as follows: the training set covered the period from 1993.0 to 2012.9, the validation set from 2013.0 to 2015.9, and the test set from 2016.0 to 2020.9. This split was chosen to ensure sufficient training data and to align with the daily resolution of the dataset over integer years. The specific parameter settings are presented in Table 5.

We employed the ANN, GRU, and LSTM models to predict SA time series and to explore the differences in the prediction results of the various deep learning models under the fluctuations of the SA time series at different virtual stations. The accuracy evaluation metrics for the prediction results of each model are presented in Figure 6.

Figure 6 demonstrates that the LSTM model significantly surpassed the ANN and GRU models. Although the ANN and GRU models show some strengths across different stations, their performance was overall inferior to that of the LSTM model. Specifically, in terms of evaluation metrics, the LSTM model achieved average RMSE, MAE, and R^2 values of 48.92 mm, 35.99 mm, and 0.85 across various SA virtual stations, while the GRU and ANN models had average RMSE, MAE, and R^2 values of 58.72 mm, 41.08 mm, 0.80 and 51.40 mm, 40.56 mm, 0.84, respectively. Therefore, the LSTM model clearly outperformed the other two models.

However, the RMSE and MAE values for station 0979 were notably higher, and its R^2 was lower compared to other stations. To investigate the prediction error at station 0979, we compared its prediction results with those from station 0933. Figure 7 visualizes the prediction results for stations 0979 (a) and 0933 (b) using different models, highlighting the superior predictive performance of the LSTM model. This comparison helps illustrate that the LSTM model provides more accurate forecasts and sheds light on the performance disparities observed at station 0979.

We concluded that the LSTM model outperformed ANN and GRU in predicting overall and extreme values. Station 0979 had a higher fluctuation frequency and more noise compared with station 0933, leading to a worse prediction accuracy. To further improve prediction accuracy, incorporating data decomposition methods to extract and analyze complex time series features could be a promising approach.

4. CONCLUSIONS

In this study, we used SA re-analysis data from CMEMS and TGs from PSMSL to estimate the ASL in the China Seas and the neighboring ocean from 1993.0 to 2020.9 using the ARMA (1,1) noise model. Besides, we analyzed the consistency of two observations and explored the performance and accuracy of the ANN, GRU, and LSTM deep learning models used to predict the SA time series. Our conclusions were as follows:

1. The ASL rate in the China Seas and the neighboring ocean from 1993.0 to 2020.9 ranged from 2.81 to 4.37 mm/yr, with an average rate of 3.55 mm/yr. This result is consistent with recent studies. The rate for the East China Sea was slightly lower than that for the South China Sea,

Table 5 Hyperparameter settings for ANN, GRU, and LSTM models.

Model	ANN	GRU	LSTM	Instructions
Training set	7305	7305	7305	Training data for model training (1993–2012)
Validation set	1095	1095	1095	Validation data to tune the hyperparameters and prevent overfitting (2013–2015)
Test set	1827	1827	1827	Testing data to evaluate the model's performance (2016–2020)
Epochs	50	50	50	Number of iterations of the model
Learning rate	0.001	0.001	0.001	Hyperparameter controlling the step size of the updates of the model's parameters
Input_size	1	1	1	Dimensionality of the input layer
Output_size	1	1	1	Dimensionality of the output layer
Hidden_size	256	256	256	Dimensionality of the hidden layer
Seq_len	12	12	12	Length of each sliding data window
Batch_size	16	16	16	Batch size for one-time input in the time series data

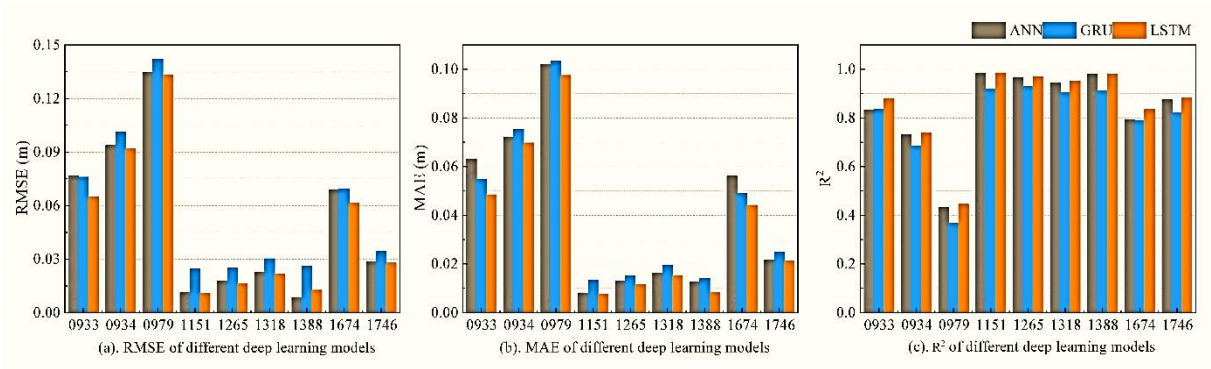

Fig. 6 Comparison of the RMSE (a), MAE (b), and R^2 (c) results from different prediction models.

as well as being lower than the mean rate along the Chinese coast (3.40 mm/yr; China Sea Level Bulletin, 2021), with a higher spatial distribution pattern in the south and a lower spatial distribution pattern in the north.

2. By combining the TG with co-located GNSS, the ASL rate in the China Seas and the neighboring ocean during the 28 years analyzed in this study was calculated to be 3.77 ± 1.05 mm/yr. The ASL rate obtained from the SA virtual stations was consistent with existing research results (He et al., 2022; Bruni et al., 2022).
3. We evaluated the prediction performance of the ANN, GRU, and LSTM models for the SA time series. The results revealed that the LSTM model outperformed the other models and achieved the highest prediction accuracy, with average RMSE, MAE, and R^2 values of 48.92 mm, 35.99 mm, and 0.85, respectively.

ACKNOWLEDGMENTS

The TG datasets are available at https://psmsl.org/. SA re-analysis data "GLOBAL_MULTIYEAR_PHY_001_030" were downloaded from https://data.marine.copernicus.eu/product/GLOBAL_MULTIYEAR_PHY_001_030/description. This work was sponsored by the National Natural Science Foundation of China (42364002) and by the Major Discipline Academic and Technical Leaders Training Program of Jiangxi Province (20225BCJ23014).

REFERENCES

Ablain, M., Legeais, J.F., Prandi, P. et al.: 2017, Satellite altimetry–based sea level at global and regional scales. Surv. Geophys., 38, 1, 7–31. DOI: 10.1007/s10712–016–9389–8

Argus, D.F., Peltier, W.R., Drummond, R. and Moore, A.W.: 2014, The Antarctica component of postglacial rebound model ICE–6G_C (VM5a) based on GPS positioning, exposure age dating of ice thicknesses, and relative sea level histories. Geophys. J. Int., 198,1, 537–563. DOI: 10.1093/gji/ggu140

Aulicino, G., Cotroneo, Y., Ruiz, S. et al.: 2018, Monitoring the Algerian Basin through glider observations, satellite altimetry and numerical simulations along a SARAL/AltiKa track. J. Marine Syst., 179, 55–71. DOI: 10.1016/j.jmarsys.2017.11.006

Balogun, A.L. and Adebisi, N.: 2021, Sea level prediction using ARIMA, SVR and LSTM neural network: assessing the impact of ensemble Ocean–Atmospheric processes on models' accuracy. Geomat. Nat. Haz. Risk, 12, 1, 653–674. DOI: 10.1080/19475705.2021.1887372

Bos, M.S., Williams, S.D.P., Araújo, I.B. and Bastos, L.: 2014, The effect of temporal correlated noise on the sea level rate and acceleration uncertainty. Geophys. J. Int., 196, 3,1423–1430. DOI: 10.1093/gji/ggt481

Bruni, S., Fenoglio, L., Raicich, F. and Zerbini, S.: 2022, On the consistency of coastal sea–level measurements in the Mediterranean Sea from tide gauges and satellite radar altimetry. J. Geod., 96, 6, 41. DOI: 10.1007/s00190–022–01626–9

Cahuantzi, R., Chen, X. and Güttel, S.: 2023, A comparison of LSTM and GRU networks for learning symbolic

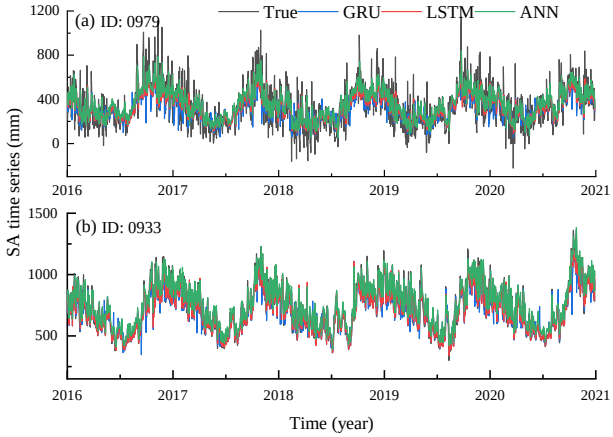

Fig. 7 Original and predicted SA time series at virtual stations 0979 (a) and 0933 (b).

sequences. In: Science and Information Conference, 771–785. Cham: Springer Nature Switzerland. DOI: 10.1007/978–3–031–37963–5_53

Cantelon, J.A., Guimond, J.A., Robinson, C.E., Michael, H.A. and Kurylyk, B.L.: 2022, Vertical saltwater intrusion in coastal aquifers driven by episodic flooding: a review. Water Resour. Res., 58, 11, e2022WR032614. DOI: 10.1029/2022WR032614

Cazenave, A. and Cozannet, G.L.: 2014, Sea level rise and its coastal impacts. Earth's Futur., 2, 2, 15–34. DOI: 10.1002/2013EF000188

Cazenave, A. and Moreira, L.: 2022, Contemporary sea–level changes from global to local scales: A review. Proc. R. Soc. A – Math. Phys. Sci., 478, 2261, 20220049. DOI: 10.1098/rspa.2022.0049

Cazenave, A. and Nerem, R.S.: 2004, Present–day sea level change: Observations and causes. Rev. Geophys., 42, 3. DOI: 10.1029/2003RG000139

Cazenave, A. and Remy, F.: 2011, Sea level and climate: measurements and causes of changes. WIRES Clim. Change, 2, 5, 647–662. DOI: 10.1002/wcc.139

Chen, H., Lu, T., Huang, J., He, X. and Sun, X.: 2023, An improved VMD–EEMD–LSTM time series hybrid prediction model for sea surface height derived from satellite altimetry data. J. Mar. Sci. Eng., 11, 12, 2386. DOI: 10.3390/jmse11122386

Chen, J., Tapley, B., Save, H. et al.: 2018, Quantification of ocean mass change using gravity recovery and climate experiment, satellite altimeter, and Argo floats observations. J. Geophys. Res., Solid Earth, 123, 11, 10,212–10,225. DOI: 10.1029/2018JB016095

China Sea Level Bulletin 2021: 2022, Ministry of Natural Resources of China. https://www.nmdis.org.cn/hygb/zghpmgb/2021nzghpmgb/

Cho, K., Van Merriënboer, B., Gulcehre, C., Bahdanau, D., Bougares, F., Schwenk, H. and Bengio, Y.: 2014, Learning phrase representations using RNN encoder–decoder for statistical machine translation. arXiv, 1406.1078. DOI: 10.48550/arXiv.1406.1078

Church, J.A. and White, N.J.: 2011, Sea–level rise from the late 19th to the early 21st century. Surv. Geophys., 32, 585–602. DOI: 10.1007/s10712–011–9119–1

Cipollini, P., Calafat, F.M., Jevrejeva, S., Melet, A. and Prandi, P.: 2017, Monitoring sea level in the coastal zone with satellite altimetry and tide gauges. Integrative study of the mean sea level and its components, 35–59. DOI: 10.1007/978–3–319–56490–6_3

Cui, Q., Xie, W. and Liu, Y.: 2018, Effects of sea level rise on economic development and regional disparity in China. J. Clean. Prod., 176, 1245–1253. DOI: 10.1016/j.jclepro.2017.11.165

Dey, R. and Salem, F.M.: 2017, Gate–variants of gated recurrent unit (GRU) neural networks. In: 2017 IEEE 60th International Midwest Symposium on Circuits and Systems (MWSCAS), 1597–1600. IEEE. DOI: 10.1109/MWSCAS.2017.8053243

Douglas, B.C.: 2001, Sea level change in the era of the recording tide gauge. Int. Geophys., 75, 37–64. DOI: 10.1016/S0074–6142(01)80006–1

Faisal, A.F., Rahman, A., Habib, M.T.M., Siddique, A.H., Hasan, M. and Khan, M.M.: 2022, Neural networks based multivariate time series forecasting of solar radiation using meteorological data of different cities of Bangladesh. Results Eng., 13, 100365. DOI: 10.1016/j.rineng.2022.100365

Feng, W., Zhong, M. and Xu, H.: 2012, Sea level variations in the South China Sea inferred from satellite gravity, altimetry, and oceanographic data. Sci. China Earth Sci., 55, 1696–1701. DOI: 10.1007/s11430–012–4394–3

Global Ocean Physics Reanalysis. E.U. Copernicus Marine Service Information (CMEMS): 2023, Marine Data Store (MDS). DOI: 10.48670/moi–00021

Guo, J.Y., Wang, J.B., Hu, Z.B., Hwang, C., Chen, C.F. and Gao, Y.G.: 2015, Temporal–spatial variations of sea level over China seas derived from altimeter data of TOPEX/Poseidon, Jason–1 and Jason–2 from 1993 to 2012. Chin. J. Geophys., 58, 9, 3103–3120. DOI: 10.6038/cjg20150908

He, X., Montillet, J.P., Fernandes, R., Melbourne, T.I., Jiang, W. and Huang, Z.: 2022, Sea level rise estimation on the Pacific coast from southern California to Vancouver Island. Remote Sens., 14, 17, 4339. DOI: 10.3390/rs14174339

Hochreiter, S. and Schmidhuber, J.: 1997, Long short–term memory. Neural Comput., 9, 8, 1735–1780. DOI: 10.1162/neco.1997.9.8.1735

Holgate, S.J., Matthews, A., Woodworth, P.L. et al.: 2013, New data systems and products at the permanent service for mean sea level. J. Coast. Res., 29, 3, 493–504. DOI:10.2112/JCOASTRES–D–12–00175.1

Houston, J.R. and Dean, R.G.: 2012, Comparisons at tide–gauge locations of glacial isostatic adjustment predictions with global positioning system measurements. J. Coast. Res., 28, 4, 739–744. DOI: 10.2112/JCOASTRES–D–11–00227.1

Hua, Y., Zhao, Z., Li, R., Chen, X., Liu, Z. and Zhang, H.: 2019, Deep learning with long short–term memory for time series prediction. IEEE Commun. Mag., 57, 6, 114–119. DOI: 10.1109/MCOM.2019.1800155

Huang, J., He, X., Montillet, J.P., Bos, M.S. and Hu, S.: 2024, Enhancing sea level rise estimation and uncertainty assessment from satellite altimetry through spatiotemporal noise modeling. Remote Sens., 16, 8, 1334. DOI: 10.3390/rs16081334

Jin, Y., Zhang, X., Church, J.A. and Bao, X.: 2021, Projected sea level changes in the marginal seas near China based on dynamical downscaling. J. Clim., 34, 17, 7037–7055. DOI: 10.1175/JCLI–D–20–0796.1

Li, Y., Wei, H., Han, Z., Huang, J. and Wang, W.: 2020, Deep learning-based safety helmet detection in engineering management based on convolutional neural networks. Adv. Civ. Eng., 1, 9703560. DOI: 10.1155/2020/9703560

LeCun, Y., Bengio, Y. and Hinton, G.: 2015, Deep learning. Nature, 521, 7553, 436–444. DOI: 10.1038/nature14539

Marcos, M., Wöppelmann, G., Matthews, A. et al.: 2019, Coastal sea level and related fields from existing observing systems. Surv. Geophys., 40, 1293–1317. DOI: 10.1007/s10712–019–09569–1

Marfai, M.A. and King, L.: 2008, Potential vulnerability implications of coastal inundation due to sea level rise for the coastal zone of Semarang city, Indonesia. Environ. Geol., 54, 1235–1245. DOI: 10.1007/s00254–007–0906–4

Montillet, J.P., Melbourne, T.I. and Szeliga, W.M.: 2018, GPS vertical land motion corrections to sea-level rise estimates in the Pacific Northwest. J. Geophys. Res., Oceans, 123, 2, 1196–1212. DOI: 10.1002/2017JC013257

Mu, D., Xu, T. and Yan, H.: 2024, Sea level rise along China coast from 1950 to 2020. Sci. China Earth Sci., 1–9. DOI: 10.1007/s11430–023–1240–x

Peltier, W.R.: 2001, Global glacial isostatic adjustment and modern instrumental records of relative sea level history. Int. Geophys., 75, 65–95. DOI: 10.1016/S0074–6142(01)80007–3

Peltier, W.R., Argus, D.F. and Drummond, R.: 2015, Space geodesy constrains ice age terminal deglaciation: The global ICE-6G_C (VM5a) model. J. Geophys. Res., Solid Earth, 120, 1, 450–487. DOI: 10.1002/2014JB011176

Permanent Service for Mean Sea Level (PSMSL): 2023, Tide gauge data. Retrieved 10 Jul 2023 from http://www.psmsl.org/data/obtaining/.

Pirani, M., Thakkar, P., Jivrani, P., Bohara, M.H. and Garg, D.: 2022, A comparative analysis of ARIMA, GRU, LSTM and BiLSTM on financial time series forecasting. In: 2022 IEEE International Conference on Distributed Computing and Electrical Circuits and Electronics (ICDCECE), 1–6. IEEE. DOI: 10.1109/ICDCECE53908.2022.9793213

Pugh, D: 2014, Sea–level science: Understanding tides, surges, tsunamis and mean sea–level changes. Cambridge University Press, 395 pp.

Qu, Y., Jevrejeva, S., Jackson, L.P. and Moore, J.C.: 2019, Coastal sea level rise around the China Seas. Global Planet. Change, 172, 454–463. DOI: 10.1016/j.gloplacha.2018.11.005

Royston, S., Watson, C.S., Legrésy, B., King, M.A., Church, J.A. and Bos, M.S.: 2018, Sea–level trend uncertainty with Pacific climatic variability and temporally–correlated noise. J. Geophys. Res., Oceans, 123, 3, 1978–1993. DOI: 10.1002/2017JC013655

Rumelhart, D.E., Hinton, G.E. and Williams, R.J.: 1986, Learning representations by back–propagating errors. Nature, 323, 6088, 533–536. DOI: 10.1038/323533a0

Saini, U., Kumar, R., Jain, V. and Krishnajith, M.U.: 2020, Univariant time series forecasting of agriculture load by using LSTM and GRU RNNs. In: 2020 IEEE Students Conference on Engineering and Systems (SCES), 1–6. IEEE. DOI: 10.1109/SCES50439.2020.9236695

Santamaría–Gómez, A., Gravelle, M. and Wöppelmann, G.: 2014, Long–term vertical land motion from double–differenced tide gauge and satellite altimetry data. J. Geod., 88, 207–222. DOI: 10.1007/s00190–013–0677–5

Schneider, T.: 2001, Analysis of incomplete climate data: Estimation of mean values and covariance matrices and imputation of missing values. J. Clim., 14, 5, 853–871. DOI: 10.1175/1520–0442(2001)014

Song, X., Liu, Y., Xue, L., Wang, J., Zhang, J., Wang, J., Jiang, L. and Cheng, Z.: 2020, Time–series well performance prediction based on Long Short–Term Memory (LSTM) neural network model. J. Petrol. Sci. Eng., 186, 106682. DOI: 10.1016/j.petrol.2019.106682

Sun, Q., Wan, J. and Liu, S.: 2020, Estimation of sea level variability in the China Sea and its vicinity using the SARIMA and LSTM models. IEEE J. Sel. Top. Appl. Earth Obs. Remote Sens., 13, 3317–3326. DOI: 10.1109/JSTARS.2020.2997817

Tong, Z., Yong–Qiang, Y.U., Cun–De, X.I.A.O., Li–Juan, H.U.A. and Zhan, Y.A.N.: 2022, Interpretation of IPCC AR6 report: monitoring and projections of global and regional sea level change. Adv. Clim. Chang. Res., 18, 1, 12. DOI: 10.12006/j.issn.1673–1719.2021.231

Wang, J., Church, J.A., Zhang, X., Gregory, J.M., Zanna, L. and Chen, X.: 2021, Evaluation of the local sea-level budget at tide gauges since 1958. Geophys. Res. Lett., 48, 20, 2021GL094502. DOI: 10.1029/2021GL094502

Wang, H., Li, W. and Xiang, W.: 2022a, Sea level rise along China coast in the last 60 years. Acta Oceanol. Sin., 41, 12, 18–26. DOI: 10.1007/s13131–022–2066–5

Wang, F., Shen, Y., Chen, Q. and Geng, J.: 2022b, Revisiting sea–level budget by considering all potential impact factors for global mean sea–level change estimation. Sci. Rep., 12, 1, 10251. DOI: 10.1038/s41598–022–14173–2

Woodworth, P.L. and Player, R.: 2003, The permanent service for mean sea level: An update to the 21st Century. J. Coast. Res., 287–295.

Wöppelmann, G. and Marcos, M.: 2016, Vertical land motion as a key to understanding sea level change and variability. Rev. Geophys., 54, 1, 64–92. DOI: 10.1002/2015RG000502

Yu, Y., Si, X., Hu, C. and Zhang, J. : 2019, A review of recurrent neural networks: LSTM cells and network architectures. Neural Comput., 31, 7, 1235–1270. DOI: 10.1162/neco_a_01199

Yuan, J., Guo, J., Zhu, C., Hwang, C., Yu, D., Sun, M. and Mu, D.: 2021, High–resolution sea level change around China seas revealed through multi–satellite altimeter data. Int. J. Appl. Earth Obs. Geoinf., 102, 102433. DOI: 10.1016/j.jag.2021.102433

Zhou, D., Liu, Y., Feng, Y., Zhang, H., Fu, Y., Liu, Y. and Tang, Q.: 2022, Absolute sea level changes along the coast of China from tide gauges, GNSS, and satellite altimetry. J. Geophys. Res., Oceans, 127, 9, 2022JC018994. DOI: 10.1029/2022JC018994